

Limpets counteract ocean acidification induced shell corrosion by thickening of aragonitic shell layers

Gerald Langer¹, Gernot Nehrke², Cecilia Baggini³, Riccardo Rodolfo-Metalpa⁴, Jason Hall-Spencer³,

5 Jelle Bijma²

¹Department of Earth Sciences, Cambridge University, Cambridge, UK

²Biogeosciences, Alfred Wegener Institute, Bremerhaven, Germany

³School of Marine Science and Engineering, University of Plymouth, Plymouth, UK

10 ⁴CoRéUs, Institut de Recherche pour le Développement, Centre IRD de Noumea, Noumea, New Caledonia

ABSTRACT

Specimens of the patellogastropod limpet *Patella caerulea* were collected within (pH_{low}-shells) and outside (pH_n-shells) a CO₂ vent site at Ischia, Italy. Four pH_{low}-shells and
15 four pH_n-shells were sectioned transversally and scanned for polymorph distribution by means of confocal Raman microscopy. The pH_{low}-shells displayed a twofold increase in aragonite area fraction and size normalised aragonite area. Size normalised calcite area was halved in pH_{low}-shells. Taken together with the increased apical and the decreased flank size normalised thickness of the pH_{low}-shells, these data led us to conclude that low pH exposed *P.*
20 *caerulea* specimens counteract shell dissolution by enhanced shell production. The latter is different from normal elongation growth and proceeds through addition of aragonitic parts only, while the production of calcitic parts is confined to elongation growth. Therefore aragonite cannot be regarded as a per se disadvantageous polymorph under ocean acidification conditions.

1. INTRODUCTION

There is general consensus that anthropogenic CO₂ emissions lead to decreasing surface ocean pH and carbonate ion concentration, a process termed ocean acidification (e.g. Royal Society, 2005). The latter entails a decrease in seawater saturation state with respect to calcium carbonate. Calcium carbonates occur in the form of different polymorphs, the most resistant to dissolution being calcite, followed by aragonite. It was proposed that by the year 2100 the subarctic Pacific Ocean and the entire Southern Ocean will be under-saturated with respect to aragonite (Orr et al., 2005). Wintertime aragonite under-saturation in the Southern Ocean may even occur as early as 2030 (McNeil and Matear, 2008). Since many marine organisms use aragonite or calcite to build their shells, there have been concerns regarding the vulnerability of these organisms to ocean acidification. The fact that aragonite is more soluble than calcite has led to the widely held notion that aragonite producers are more vulnerable to ocean acidification than calcite producers (Field et al., 2011; Gattuso and Hansson, 2011; Royal Society, 2005). The extreme sensitivity of aragonitic pteropods to dissolution (Bednarsek et al., 2012) seems to support this view. Some molluscs, e.g. patellogastropod limpets and the Littorinidae (Hedegaard et al., 1997; Taylor and Reid, 1990), have, in addition to aragonitic shell layers, evolved outer calcitic shell layers. It was argued that calcitic shell layers are an adaptation to resist dissolution (Taylor and Reid, 1990). The latter hypothesis was questioned on the basis of a comparative dissolution study using aragonitic and calcitic bivalve microstructures (Harper, 2000). Comparing the post-mortem dissolution rates of four (two aragonitic and two calcitic) Antarctic benthic species, McClintock et al. (2009) supported the conclusion of Harper (2000). The latter two studies imply the notion that dissolution of calcium carbonate biominerals is not primarily a question of the polymorph, but depends largely on composition and microstructure of the biomineral. As regards the vulnerability to ocean acidification, shell dissolution is merely one aspect, which focuses

entirely on the product, i.e. the shell. The production of the latter is another aspect, and under ocean acidification some organisms might be able to compensate for shell dissolution by increasing shell production (Rodolfo-Metalpa et al., 2011). This compensatory shell production might favour the more dissolution resistant polymorph in species producing both aragonite and calcite (see also Taylor and Reid, 1990). Specimens of the limpet *Patella caerulea*, collected at a highly acidified volcanic CO₂ vent site at Ischia, displayed higher gross calcification rates than their fellow specimens, collected outside the vent site (normal pH, Rodolfo-Metalpa et al., 2011). It was also shown that *P. caerulea* specimens collected within the vent site are considerably corroded (Hall-Spencer et al., 2008; Rodolfo-Metalpa et al., 2011). Taken together the latter two observations suggest that *P. caerulea* might be able to compensate, to a certain extent (compare Hall-Spencer et al., 2008; Rodolfo-Metalpa et al., 2011), shell dissolution by excess shell production. Since limpets produce aragonitic as well as calcitic shell layers (see above), an interesting question is whether compensatory shell production shows a bias towards a particular polymorph. Here we present the polymorph distribution of complete cross sections of *P. caerulea* shells collected from within and outside the Ischia CO₂ vent site (Hall-Spencer et al., 2008; Rodolfo-Metalpa et al., 2011).

2. MATERIAL AND METHODS

2.1. Study site and sampling

The study site is an area located off the east coast of Ischia (40°43.81'N, 13°57.98'E), in shallow waters of 2-6 m and within 1-15 m of the shore line. Emissions from the vents in this area are composed of 90–95% CO₂, 3–6% N₂, 0.6–0.8% O₂, 0.2–0.8% CH₄ and 0.08–0.1% Ar, without toxic sulphur compounds (Hall-Spencer et al., 2008). Since the vent gases do not contain toxic substances and are at ambient seawater temperature, this area can be used as a

75 natural laboratory to understand ecosystem effects of ocean acidification. Gas fluxes were measured during 2006-2007, and no seasonal, tidal or diurnal variation in gas flow rates was detected, while pH and saturation states of aragonite and calcite varied with sea state, being lowest on calm days, and showed large decreases as pCO₂ amounts increased proceeding towards the vent sites (Hall-Spencer *et al.*, 2008). *Patella caerulea* specimens (for
80 photographs see Figure S1) were collected from two low pH sites (PL1 and PL2), and from a control site (C) in December 2009 (Figure 1). Temperature, pH and TA were measured from September to December 2009, and the other carbonate chemistry parameters were calculated from them. PL1 and PL2 had a mean pH of 6.46 ± 0.35 (mean \pm S.D.) and 6.51 ± 0.38 respectively, while the control site had a mean pH of 8.03 ± 0.05 (Table 1).

85

2.2. Sample preparation and Raman spectroscopy:

Raman imaging was done using a WITec alpha 300 R (WITec GmbH, Germany) confocal Raman microscope. Imaging was done using a motorized scan table having a maximum scan range of up to 2.5 x 2.5 cm and a minimum step size of 100 nm. Scans are
90 performed using a 532 nm diode laser and an ultra-high throughput spectrometer with a grating, 600/mm, and 500 mm blaze (UHTS 300, WITec, Germany). The used objective was a 20x Zeiss with a NA of 0.4.

For the imaging every 10 μm a Raman spectra was acquired with a integration time of 0.05 s per spectra. The size of the sample and its irregular shape as well as the extremely high
95 resolution of 10 μm (resulting in huge spectral files) did not allow imaging the whole sample in one run. Therefore the sample had to be repositioned several times. Therefore the sample processing had to be done for each scan separately (using the WITec Project software, version 2.10). This resulted in slightly different colour scales for each image, since it was not possible

to synchronize the latter during the data processing. However, this does only alter the optical
100 appearance of the images after they have been stitched together using the software Gimp 2.8
and does not affect the interpretation of the images. For details on the Raman imaging of this
type of samples the interested reader is referred to several other publications performed using
the described setup (e.g. Nehrke and Nouet, 2011; Nehrke et al., 2012; Wall and Nehrke,
2012; Stemmer and Nehrke 2014).

105

2.3. Size measurements and data analysis

Transversally sectioned and resin-embedded shells were imaged using a Nikon
SMZ1500 stereo microscope. Shell length and shell thickness were measured using Nikon
NIS Elements 4.0 software. All bar-plots show the mean \pm standard deviation of four shells
110 (four pH_{low}-shells and four pH_n-shells were analysed). Since shells of *P.caerulea* are not
symmetric we always measured the shorter of the two shell flanks. Size normalised thickness
of a shell's shorter flank (SNTF) was determined by averaging ca. 35 evenly spaced thickness
measurements and dividing the resulting value by the shell's length. Size normalised thickness
of a shell's apex (SNTA) was determined by averaging ca. 10 evenly spaced thickness
115 measurements and dividing the resulting value by the shell's length. The apex of a shell was
arbitrarily defined as a certain distance (ca. 1.5 mm) left and right to the highest point of the
shell (see Figure 2). The latter measure was taken to avoid a one-point measurement of the
highest point of a shell. Such a one-point measurement is prone to being not representative.
The fraction of aragonite area (FA) was determined as pixels representing aragonite
120 (measured by means of Nikon NIS Elements 4.0 software) divided by the sum of pixels
representing aragonite and pixels representing calcite (Figure 3). The size normalised
aragonite area (SNAA) equals pixels representing aragonite divided by the shell length. The

size normalised calcite area (SNCA) equals pixels representing calcite divided by the shell length.

125

3. RESULTS

All shells selected for analysis were of similar size. The length of the pH_n -shells was 31 ± 2 mm (mean \pm standard deviation of four shells), while the length of the pH_{low} -shells was 36 ± 3 mm (mean \pm standard deviation of four shells). Polymorph distribution imaging revealed marked differences between pH_{low} -shells and pH_n -shells (Figure 4). Size normalised thickness of the flank (SNTF) was 26% lower in pH_{low} -shells (Figure 5), while size normalised thickness of the apex (SNTA) was 26% higher in pH_{low} -shells (Figure 6). The fraction of aragonite area (FA) was by a factor of 2.3 higher in pH_{low} -shells (Figure 7). Size normalised aragonite area (SNAA) was by a factor of 2.2 higher in pH_{low} -shells (Figure 8), and size normalised calcite area (SNCA) was by a factor of 2.4 lower in pH_{low} -shells (Figure 9).

130
135

4. DISCUSSION

The low pH site at Ischia, from which the analysed pH_{low} -shells were taken, features seawater that is under-saturated with respect to both aragonite and calcite (Table 1). Hence shells of calcareous organisms residing in these under-saturated waters are prone to dissolution. Indeed, shells of *P. caerulea* clearly show signs of dissolution (Hall-Spencer et al., 2008; Rodolfo-Metalpa et al., 2011). Therefore, *P. caerulea* pH_{low} -shells are the product of both shell formation and dissolution, as opposed to N-shells (originating from the normal pH site), which are merely the product of shell formation. Provided they grow normally, pH_{low} -shells should, because of dissolution, display a reduced size normalized thickness

140
145

(SNT). This is, for the flank area of the shell, indeed the case (Figure 7). On the contrary, in the apex area, the SNT is higher in pH_{low}-shells (Figure 6). The latter can only stem from enhanced shell production. From the above it can be concluded that net shell production in
150 pH_{low}-shells is region-specific, i.e. enhanced at the apex area, and reduced along the flank area. A comparison of the mineralogical composition of the shells from the two different sites shows that the fraction of aragonite area (FA) for pH_{low}-shells is twice as big as for pH_n-shells (Figure 7). This observation could exclusively be due to a higher SNT of the apex area, which is predominantly aragonitic. If the increased FA is related to normal shell production and
155 dissolution, the size normalised aragonite area (SNAA) should be unaltered or decreased. We observed, contrariwise, an increased SNAA (Figure 8), which is in line with the increased SNT of the apex area, both pointing to enhanced shell production. Along the flank area, however, the SNT is decreased in pH_{low}-shells (Figure 7), and so is the overall size normalised calcite area (SNCA, Figure 9). To conclude, there is ample evidence suggesting
160 that low pH exposed *P. caerulea* specimens counteract dissolution by enhanced shell production. Hence the mineralogical analyses of the shell sections support our conclusion drawn on the basis of the thickness measurements, i.e. that enhancement of shell production is region-specific, and, by entailment, polymorph-specific. The latter conclusion is plausible when considering simultaneous shell growth and dissolution as will be detailed in the
165 following.

Under normal pH conditions *P. caerulea* produces shells characterized by a predominately aragonitic apex area and a flank area which is aragonitic and calcitic in the upper part but solely calcitic in the lower part. This is different for shells formed under low pH conditions. The apex area is still predominantly aragonitic but large parts of the flank area
170 are now aragonitic as well (compare Figure 4). This observation is related to the fact that shell growth and dissolution take place simultaneously during the complete lifespan of *P. caerulea*.

Under normal pH conditions the shell is growing by the addition of calcitic material at the edges of the shell flank in form of a cross foliated structure (MacClintock, 1967). With time this material is dissolved which results in a thinning of the shell. Our observations suggest that *P. caerulea* counteracts this thinning by depositing additional layers on the inner side of the shell. Since the deposition of layers at the inner side of the shell is related to a mechanism producing aragonite the amount of aragonite increases while calcitic parts at the outside are dissolved. New formation of calcitic areas is only possible during elongation of the shell (increase in size) but not to counteract dissolution. The scenario described above results in the relative (as expressed by FA, Figure 7) increase in aragonite in the pH_{low}-shells. Taken together with the absolute (as expressed by SNAA, Figure 8) increase in aragonite and the increased SNT of the apex area (Figure 6) in the pH_{low}-shells, this suggests a high efficacy of the compensatory shell production. Our results demonstrate that the ability of limpets to cope, to a certain extent (compare also Hall-Spencer et al., 2008; Rodolfo-Metalpa et al., 2011), with corrosive waters is not related to the preferential usage of the more dissolution resistant polymorph, but is solely governed by the mechanism of shell formation. This mechanism allows for compensatory shell thickening through the deposition of additional layers on the inner side of the shell. We do not know whether the additional layers are structural layers. One possibility is that the layers we call “additional” are similar to the layers related to shell repair in *Haliotis* (Fleury et al. 2008). These additional layers are aragonitic, but this is genetically determined and does not represent a response to ocean acidification. The shift towards aragonite seen in pH_{low}-shells is simply a by-product of the way limpets use calcium carbonate polymorphs in shell formation. The fact that the additional, aragonitic, layers of the pH_{low}-shells lead to an increased SNT of the apex (Figure 6) also shows that aragonite cannot be regarded as a per se disadvantageous polymorph under corrosive ocean acidification. We ascribed the changes in shell mineralogy and shell thickness of our samples to seawater carbonate chemistry changes. Since these are field samples, as opposed to experimental

samples, possible secondary influences have to be considered. For *Mytilus* it was shown that maybe salinity, but certainly temperature influences the aragonite/calcite ratio (Dodd 1966, Eisma 1966). The latter is also true for *Patella* (Cohen and Branch 1992). In our case, however, both temperature and salinity at the two sites (Figure 1) were the same at any given time (Table 1, Cigliano et al. 2010, Hall-Spencer et al. 2008, Rodolfo-Metalpa et al. 2011), and we conclude that these two parameters did not influence the aragonite/calcite ratio of our samples. Also both the control site and the low pH site we sampled at Ischia are sheltered so that there is no difference in wave action, which could potentially influence shell architecture. Furthermore, it was suggested that the concentrations of inorganic ions such as Mg and Sr can influence the mineralogy of marine calcifying organisms (Watabe 1974). Since salinity was constant in our case, the concentrations of major ions such as Mg and Sr were likewise, and their influence can be ruled out. On the other hand, shells from the low pH site clearly are corroded (see above), so there is a massive impact of seawater carbonate chemistry on the organism. Taken together with the constancy of other environmental parameters, that leads us to conclude that carbonate chemistry changes are the best explanation for the changes in shell mineralogy and shell thickness of our samples.

5. Conclusion

Polymorph distribution analyses of complete cross sections of *Patella caerulea* shells from a CO₂ vent site at Ischia revealed that this species counteracts shell dissolution in corrosive waters by enhanced production of aragonitic shell layers. The question whether these layers represent structural layers will be the subject matter of an upcoming microstructural investigation.

220

Acknowledgements

No acknowledgements at this stage

References

225

Bednarsek N., Tarling G. A., Bakker D. C. E., Fielding S., Jones E. M., Venables H. J., Ward P., Kuzirian A., Leze B., Feely R. A., and Murphy E. J. (2012) Extensive dissolution of live pteropods in the Southern Ocean. *Nature Geoscience* 5(12), 881-885.

Cigliano, M; Gambi, Maria Cristina; Rodolfo-Metalpa, Riccardo; Patti, F P; Hall-Spencer, Jason M (2010): Effects of ocean acidification on invertebrate settlement at volcanic CO₂ vents. *Marine Biology*, 157(11), 2489-2502

Cohen, A.L., Branch, G.M. (1992) Environmentally controlled variation in the structure and mineralogy of *Patella granularis* shells from the coast of southern Africa: implications for palaeotemperature assessments, *Palaeogeography, Palaeoclimatology, Palaeoecology*, Volume 91, Pages 49-57

Dodd, J.R. (1966) The Influence of Salinity on Mollusk Shell Mineralogy: A Discussion. *The Journal of Geology*, Vol. 74, pp. 85-89

Eisma, D. (1966) The Influence of Salinity on Mollusk Shell Mineralogy: A Discussion. *The Journal of Geology*, Vol. 74, pp. 89-94

Field C. B., Barros V., Stocker T. F., Dahe Q., Mach K. J., Plattner G., Mastrandrea M. D., Tignor M., and Ebi K. L. (2011) IPCC Workshop on Impacts of Ocean Acidification on Marine Biology and Ecosystems, 164pp.

Fleury, C., Marin, F. Marie, B. Luquet, G. Thomas, J., Josse, C., Serpentine, A., Lebel, J.M. (2008) Shell repair process in the green ormer *Haliotis tuberculata*: A histological and microstructural study, *Tissue and Cell* 40, 207-218

Gattuso J.-P. and Hansson L. (2011) *Ocean Acidification*. Oxford University Press.

- Hall-Spencer J. M., Rodolfo-Metalpa R., Martin S., Ransome E., Fine M., Turner S. M., Rowley S. J., Tedesco D., and Buia M.-C. (2008) Volcanic carbon dioxide vents show ecosystem effects of ocean acidification. *Nature* **454**(7200), 96-99.
- 250 Harper E. M. (2000) Are calcitic layers an effective adaptation against shell dissolution in the Bivalvia? *Journal of Zoology* **251**, 179-186.
- Hedegaard C., Lindberg D. R., and Bandel K. (1997) Shell microstructure of a Triassic patellogastropod limpet. *Lethaia* **30**, 331-335.
- MacClintock, C. (1967) Shell Structure of Patelloid and Bellerophontoid Gastropods (Mollusca).
255 Peabody Museum of Natural History Yale University Bulletin 22, New Haven, Connecticut
- McClintock J. B., Angus R. A., McDonald M. R., Amsler C. D., Catledge S. A., and Vohra Y. K. (2009) Rapid dissolution of shells of weakly calcified Antarctic benthic macroorganisms indicates high vulnerability to ocean acidification. *Antarctic Science* **21**(05), 449-456.
- McNeil B. I. and Matear R. J. (2008) Southern Ocean acidification: A tipping point at 450-ppm
260 atmospheric CO₂. *Proceedings of the National Academy of Sciences* **105**(48), 18860-18864.
- Nehrke, G. and Nouet J. (2011) Confocal Raman microscope mapping as a tool to describe different mineral and organic phases at high spatial resolution within marine biogenic carbonates: case study on *Nerita undata* (Gastropoda, Neritopsina). *Biogeosciences* **8** (12): p. 3761-3769.
- Nehrke, G., Poigner H., Wilhelms-Dick D., Brey T., and Abele D. (2012) *Coexistence of three calcium carbonate polymorphs in the shell of the Antarctic clam *Laternula elliptica**. *Geochem. Geophys. Geosyst.* **13**: p. Q05014.
- 265 Orr J. C., Fabry V. J., Aumont O., Bopp L., Doney S. C., Feely R. A., Gnanadesikan A., Gruber N., Ishida A., Joos F., Key R. M., Lindsay K., Maier-Reimer E., Matear R., Monfray P., Mouchet A., Najjar R. G., Plattner G.-K., Rodgers K. B., Sabine C. L., Sarmiento J. L., Schlitzer R., Slater R. D.,
270 Totterdell I. J., Weirig M.-F., Yamanaka Y., and Yool A. (2005) Anthropogenic ocean acidification over the twenty-first century and its impact on calcifying organisms. *Nature* **437**(7059), 681-686.

- Rodolfo-Metalpa R., Houlbreque F., Tambutte E., Boisson F., Baggini C., Patti F. P., Jeffree R., Fine M., Foggo A., Gattuso J.-P., and Hall-Spencer J. M. (2011) Coral and mollusc resistance to ocean acidification adversely affected by warming. *Nature Climate Change* **1**(6), 308-312.
- 275 Royal Society (2005) Ocean acidification due to increasing atmospheric carbon dioxide, pp. 60. Policy Document 12/05, The Royal Society, London.
- Stemmer, K. and Nehrke G. (2014) *THE DISTRIBUTION OF POLYENES IN THE SHELL OF ARCTICA ISLANDICA FROM NORTH ATLANTIC LOCALITIES: A CONFOCAL RAMAN MICROSCOPY STUDY*. *Journal of Molluscan Studies* **80**, 365-370, doi:10.1093/molus/eyu033
- 280 Taylor J. D. and Reid D. G. (1990) Shell microstructure and mineralogy of the Littorinidae: ecological and evolutionary significance. *Hydrobiologia* **193**, 199-215.
- Wall, M. and Nehrke G. (2012) *Reconstructing skeletal fiber arrangement and growth mode in the coral Porites lutea (Cnidaria, Scleractinia): a confocal Raman microscopy study*. *Biogeosciences* **9**(11): p. 4885-4895.
- 285 Watabe, N. (1974) Crystal growth of calcium carbonate in biological systems, *Journal of Crystal Growth*, Volumes 24–25, Pages 116-122

TABLES

Table 1. Mean value (\pm S.D.) of temperature (T), pH (total scale), pCO₂, concentration of HCO₃⁻ and CO₃²⁻ ions, CO₂ concentration in sea water, dissolved inorganic carbon (DIC), saturation state (Ω) of aragonite and calcite for the study sites.

Site	T (°C)	pH _T	pCO ₂ (μ atm)	HCO ₃ ⁻ (μ mol/kg)	CO ₃ ²⁻ (μ mol/kg)	CO ₂ (μ mol/kg)	DIC (μ mol/kg)	Ω_{Ca}	Ω_{Ar}
C	19.7 (\pm 2.0)	8.03 (\pm 0.05)	474 (\pm 74)	2043 (\pm 46)	220 (\pm 19)	15 (\pm 2)	2279 (\pm 29)	5.15 (\pm 0.45)	3.36 (\pm 0.30)
PL1	20.1 (\pm 2.2)	6.46 (\pm 0.35)	22047 (\pm 13264)	2542 (\pm 50)	14 (\pm 21)	758 (\pm 510)	3315 (\pm 526)	0.33 (\pm 0.48)	0.22 (\pm 0.32)
PL2	20.1 (\pm 2.2)	6.51 (\pm 0.38)	19504 (\pm 12338)	2509 (\pm 96)	17 (\pm 18)	618 (\pm 392)	3143 (\pm 426)	0.39 (\pm 0.43)	0.26 (\pm 0.28)

FIGURE CAPTIONS

Figure 1. Map of the study area, showing the low pH sites (PL1 and PL2) and the control site (C).

Figure 2: Sketch of a shell indicating length, apex, and shortest flank.

Figure 3: Example of a Raman image across the cross section of the Shell. Blue represents
300 aragonite and yellow calcite, as identified by the corresponding Raman spectra shown.

Figure 4: Polymorph distribution of transversally sectioned shells. Blue = aragonite, yellow = calcite. Normal = pH_n -shells, Low = pH_{low} -shells.

Figure 5: Size normalised thickness of the flank (SNTF). Normal = pH_n -shells, Low = pH_{low} -shells.

305 Figure 6: Size normalised thickness of the apex (SNTA). Normal = pH_n -shells, Low = pH_{low} -shells.

Figure 7: Fraction of aragonite area (FA). Normal = pH_n -shells, Low = pH_{low} -shells.

Figure 8: Size normalised aragonite area (SNAA). Normal = pH_n -shells, Low = pH_{low} -shells.

Figure 9: Size normalised calcite area (SNCA). Normal = pH_n -shells, Low = pH_{low} -shells.

Figure 1

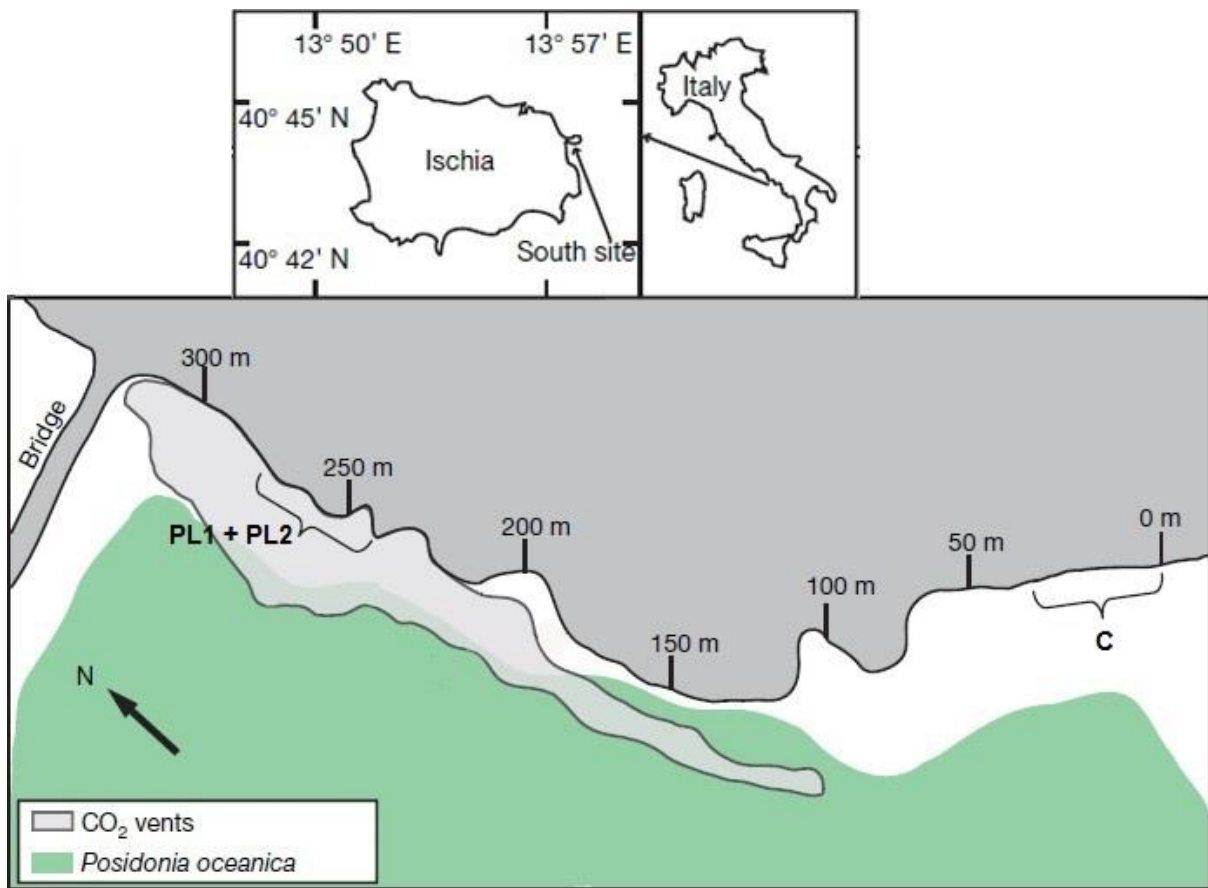
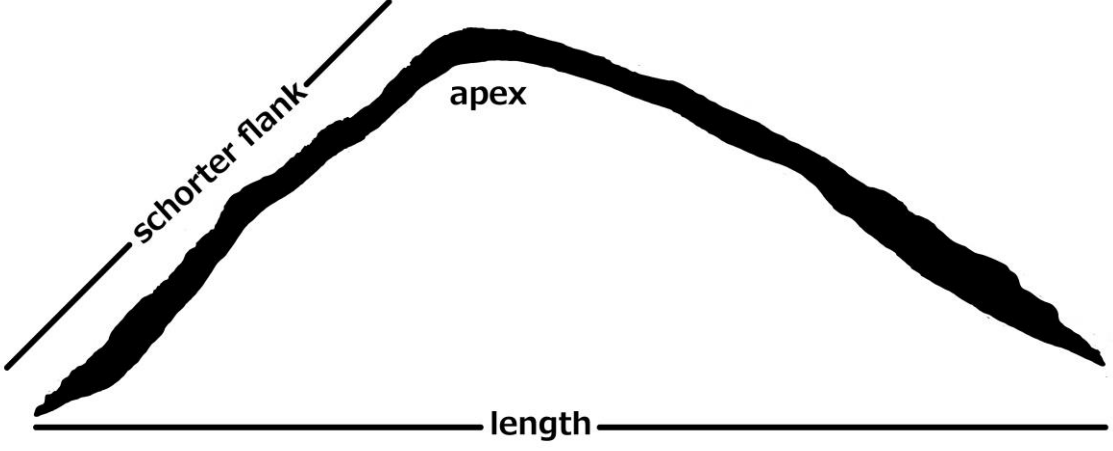
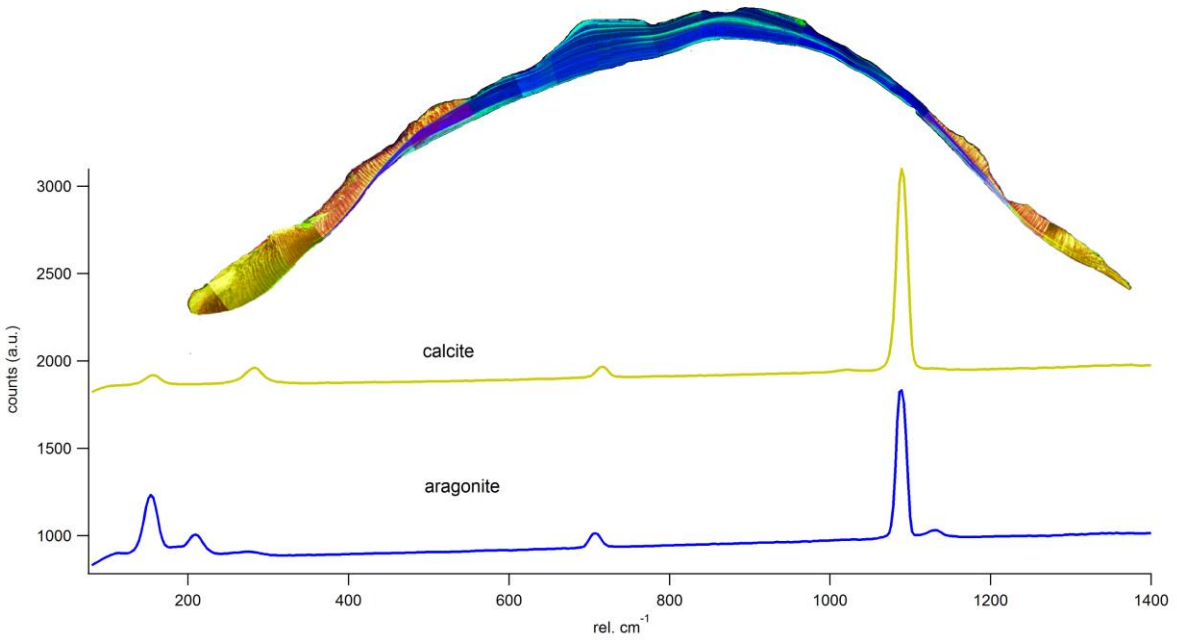


Figure 2:



315

Figure 3:



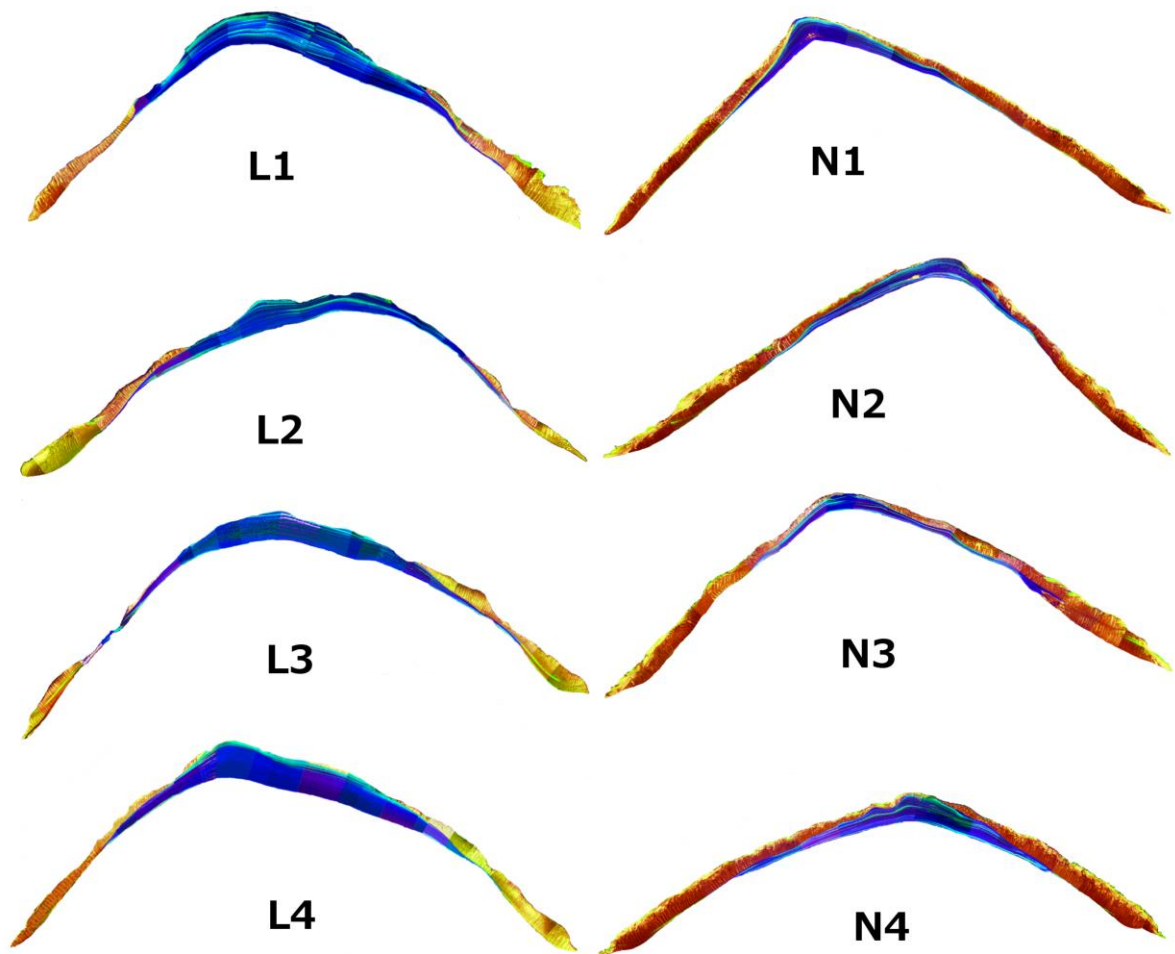


Figure 5:

325

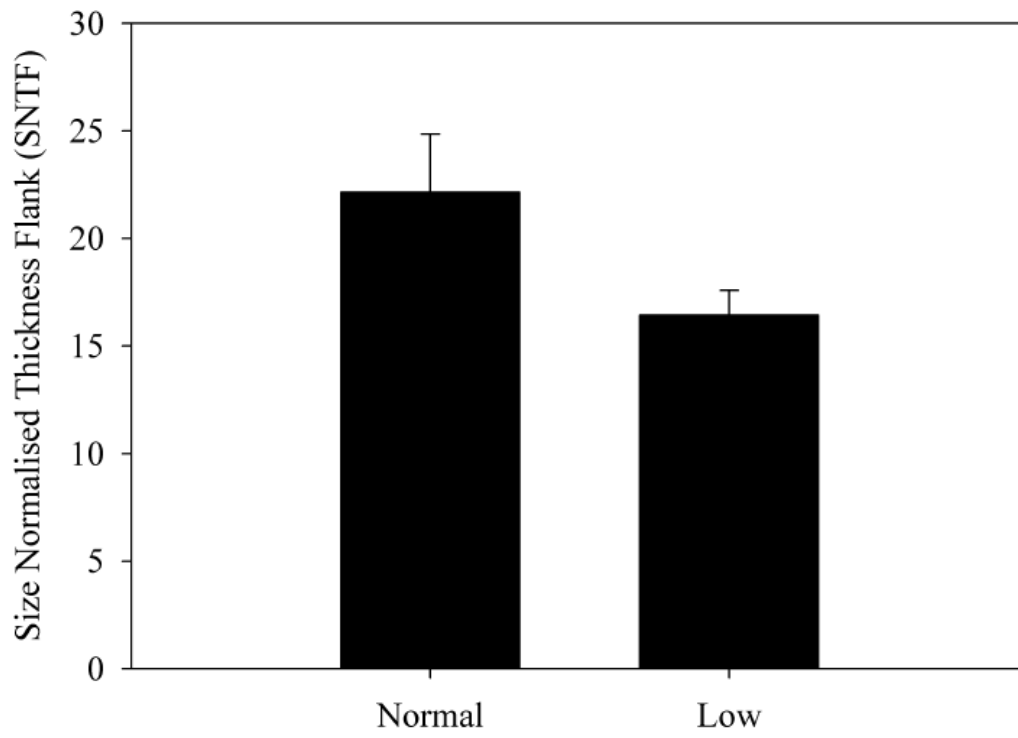
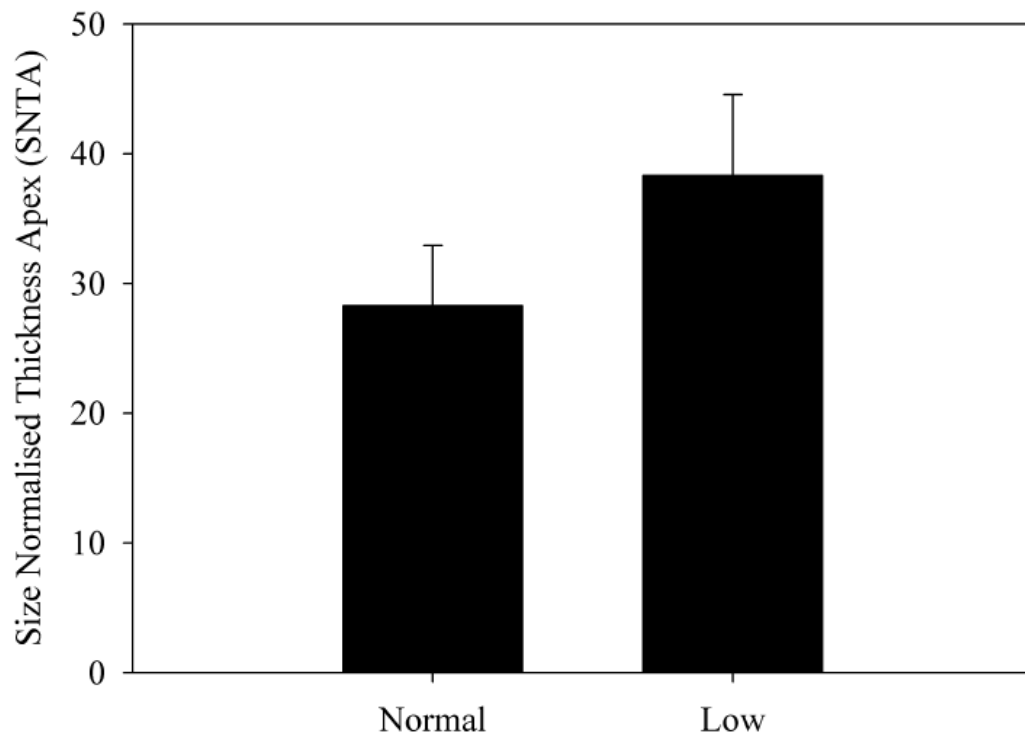
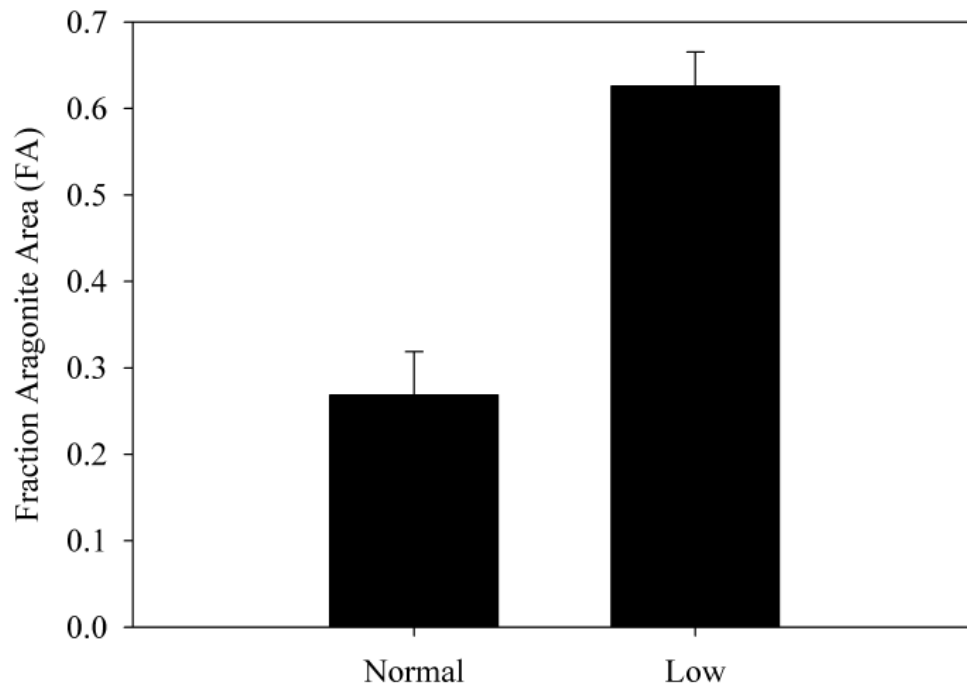


Figure 6:



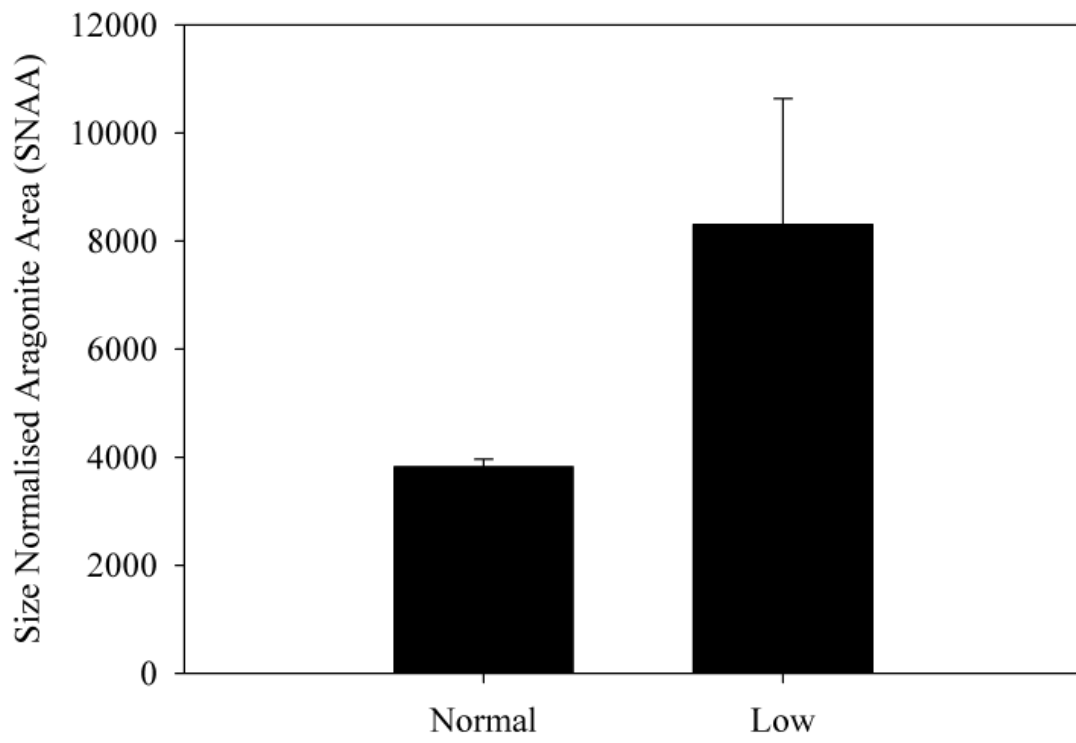
330

Figure 7:



335

Figure 8:



340 Figure 9:

